

RESEARCH ARTICLE | NOVEMBER 10 2023

Understanding why constant energy or constant temperature may affect nucleation behavior in MD simulations: A study of gas hydrate nucleation

Lei Wang  ; Peter G. Kusalik  



J. Chem. Phys. 159, 184501 (2023)

<https://doi.org/10.1063/5.0169669>



View
Online



Export
Citation

CrossMark



The Journal of Chemical Physics

Special Topic: Algorithms and Software
for Open Quantum System Dynamics

Submit Today

 AIP
Publishing

Understanding why constant energy or constant temperature may affect nucleation behavior in MD simulations: A study of gas hydrate nucleation

Cite as: J. Chem. Phys. 159, 184501 (2023); doi: 10.1063/5.0169669

Submitted: 27 July 2023 • Accepted: 18 October 2023 •

Published Online: 10 November 2023



View Online



Export Citation



CrossMark

Lei Wang and Peter G. Kusalik^{a)}

AFFILIATIONS

Department of Chemistry, University of Calgary, 2500 University Drive NW, Calgary, Alberta T2N 1N4, Canada

^{a)}Author to whom correspondence should be addressed: pkusalik@ucalgary.ca

ABSTRACT

Molecular dynamics simulations have been widely used in exploring the nucleation behavior of many systems, including gas hydrates. Gas hydrates are ice-like solids in which gas molecules are trapped in water cages. During hydrate formation, a considerable amount of heat is released, and previous work has reported that the choice of temperature control scheme may affect the behavior of hydrate formation. The origins of this effect have remained an open question. To address this question, extensive NVE simulations and thermostatted (NPT and NVT) simulations with different temperature coupling strengths have been performed and compared for systems where a water nanodroplet is immersed in a H₂S liquid. Detailed analysis of the hydrate structures and their mechanisms of formation has been carried out. Slower nucleation rates in NVE simulations in comparison to NPT simulations have been observed in agreement with previous studies. Probability distributions for various temperature measures along with their spatial distributions have been examined. Interestingly, a comparison of these temperature distributions reveals a small yet noticeable difference in the widths of the distributions for water. The somewhat reduced fluctuations in the temperature for the water species in the NVE simulations appear to be responsible for reducing the hydrate nucleation rate. We further conjecture that the NVE-impeded nucleation rate may be the result of the finite size of the surroundings (here the liquid H₂S portion of the system). Additionally, a local spatial temperature gradient arising from the heat released during hydrate formation could not be detected.

Published under an exclusive license by AIP Publishing. <https://doi.org/10.1063/5.0169669>

INTRODUCTION

Gas hydrates are ice-like inclusion compounds in which guest molecules (e.g., CH₄ and H₂S) are trapped in water hydrogen-bonded cavities.¹ Gas hydrates have attracted considerable attention because of the vast occurrence of natural methane hydrates^{2–7} and promising technological applications, such as gas storage,^{7–9} gas separation,^{7,8,10} CO₂ sequestration,^{7,8} and seawater desalination,^{7,11,12} as well as because of safety concerns arising from the formation of hydrate blockages in gas/oil pipelines.^{7,13} Relevant to these significant applications, a fundamental understanding of nucleation behavior and mechanisms is necessary to support ongoing developments associated with gas hydrates. However, due to the small length scales (nanometers) and small temporal scales

(nanoseconds) on which nucleation of clathrate hydrates occurs, the molecular behavior associated with hydrate nucleation is still exceptionally challenging for current experiments to access. Molecular dynamics (MD) simulations have therefore become regarded as a powerful tool to study nucleation mechanisms at the microscopic level.¹⁴

Aiming to achieve a better understanding of molecular behavior during nucleation, many MD studies have been devoted to the investigation of the mechanism for hydrate formation.^{15–45} Most studies have been performed under temperature-controlled conditions so that the information extracted from MD simulations can be used directly to connect to theoretical models that assume isothermal conditions. In these MD simulations,^{15–36,38,41–45} the temperature is controlled via coupling to an external bath at a specific

temperature to allow heat exchange with the system. In this way, the latent heat generated by, for example, hydrate formation can be dissipated essentially immediately through the coupling to the thermal bath. Consequently, in such studies, mass transfer then tends to be a predominant factor for determining the rate of hydrate formation.

Yet, the heat associated with hydrate formation/dissociation is non-trivial.^{1,11,46–49} For example, the enthalpy change for the dissociation of CO₂ or CH₄ hydrate is around 9.0 kJ/mol of water.^{46,50} Such a large amount of heat is sufficient to increase the temperature of the same amount of liquid water by ~120 K. Since nucleation is rather sensitive to temperature variations, any temperature increase due to the formation of hydrate nuclei could consequently be expected to suppress further nucleation events. Therefore, the possible influence of the latent heat of hydrate formation on hydrate nucleation should be investigated.

There have been only a few MD studies published exploring the influence of non-isothermal conditions (e.g., NVE simulations) during hydrate nucleation and the possible impact of latent heat on nucleation rates and nucleus structures.^{37,39,40} Liang and Kusalik³⁷ compared H₂S hydrate nucleation behavior within NPT and NVE simulations and reported that the NVE simulations exhibit a somehow slower initial nucleation rate as the latent heat released slightly warmed the local environment, while also enhancing the structural order of the hydrate nuclei with more recognizable motifs of regular hydrate crystallites. Within their NVE simulations, they observed a slight temperature increase of ~2 K at the site of the initial appearance of the hydrate nucleus in their supersaturated solutions.³⁷ In the study of Liang and Kusalik,³⁷ in which the initial system contained a small liquid H₂S droplet, NVT simulation were also performed and the authors concluded that pressure control had only a slight influence on H₂S hydrate nucleation behavior. Later, a systematic study of the influence of different ensembles on the kinetic behavior of nucleation for CH₄ hydrate formation was reported by Zhang *et al.*⁴⁰ In their study, the initial system contained a somewhat large CH₄ gas bubble immersed in an aqueous solution.⁴⁰ They found that the different ensembles can be ordered in terms of nucleation rate as NPT > NVT > NVE, but can be inversely ordered in terms of hydrate crystallinity. Given the presence of a large and highly compressible CH₄ gas bubble in their system, it is perhaps not surprising that pressure (i.e., fluctuations in pressure) might have a greater impact on hydrate nucleation.^{37,40} These two studies proposed that temperature control schemes can influence the kinetic behavior of hydrate formation. Different ensemble-dependent kinetic behavior has also been studied for other liquid scenarios (e.g., protein folding,⁵¹ polymer crystallization⁵²), as well as for nucleation in vapors.⁵³ Since the amount of heat released by nucleation in vapors is rather large, the influence of non-isothermal modelling on the nucleation rate was found to be significant.⁵³ Given that the heat released by nucleation in liquids is less than that generated by nucleation in vapors, and given the challenge of capturing local (i.e., in time and space) temperature variations within MD simulations, the question of how control of the temperature, and hence the dissipation of latent heat, may affect crystal nucleation behavior within MD simulations has remained unresolved.

In this study, we will examine how different temperature control schemes, including constant energy (designated by NVE) simulations and constant temperature simulations, may affect the nucleation of a gas hydrate system. The constant temperature

simulations include NPT simulations with different temperature coupling constants and NVT simulations with different coupling groups and different temperature control methods. The systems considered in the study consist of a water nanodroplet immersed in a H₂S liquid. It is observed that nucleation was consistently slower within the NVE simulations relative to the thermostatted simulations. Distributions for the temperature associated with different species and different regions of the system during hydrate formation are analyzed in detail. Notably, the results reveal the existence of small yet distinguishable differences in the widths of the temperature distributions for the water obtained from the thermostatted and non-thermostatted simulations. The slightly narrower distribution for non-thermostatted systems leads to the water molecules experiencing somewhat smaller fluctuations in temperature which apparently reduce the nucleation rate in comparison with thermostatted systems. We further illustrate that the appearance of such differences can be attributed to the finite size of the nanodroplet's surroundings (i.e., the H₂S liquid portion of the system). From the analysis of spatial distributions for the temperature, we were unable to detect a local temperature gradient (estimated around 0.01 K/nm) distinct from the noise in the calculations during hydrate formation in water nanodroplets.

METHODS AND ANALYSIS

Systems in which a water nanodroplet is immersed in a H₂S liquid consisting of 10 000 H₂S molecules were used in this study. Two different sizes of nanodroplets with 3000 and 4500 water molecules were considered, where the former is labelled as sys-M, and the latter is labelled as sys-L. Since the formation of gas hydrates takes place in the aqueous solution, the current system setup with a discrete water nanodroplet allows hydrate formation without the influence of periodic boundary conditions. It also allows heat exchange between the water nanodroplet (i.e., the hydrate formation region) and the surrounding bath (the H₂S liquid), thus more closely mimicking real experimental conditions with no direct control of the local temperature. The initial configurations for the production NVE trajectories were generated from a 2 ns NPT simulation with target initial temperatures, T₀, of 250 or 255 K, and a pressure of 10 MPa. Five independent NVE trajectories were then performed for sys-M with T₀ of 250 K (labelled as NVE_Mrun1–5) and with T₀ of 255 K. Five independent NVE trajectories were performed for sys-L with T₀ of 255 K, labelled as NVE_Lrun1–5. The NVE trajectories ranged from 300 to 650 ns depending on the time required for hydrate formation (see Table S1).

For comparison with the results of the NVE simulations, and to allow the analysis of the influences of temperature control schemes and temperature coupling strengths on the nucleation behavior, additional NPT simulations at 250 K were also carried out with the same methodologies except the appropriate temperature was controlled by a Nosé–Hoover thermostat,⁵⁴ and the pressure controlled by an isotropic Parrinello–Rahman barostat at 10 MPa.⁵⁵ Various temperature coupling constants (τ_T ranging from 1 to 200 ps) along with pressure coupling constants τ_P ($\tau_P = 2\tau_T$ except $\tau_P = 4$ ps for $\tau_T = 1$ ps) were used with sys-M (see Table S1), where one trajectory was performed for each τ_T and labelled as NPT_Mrun_{T_T}, accordingly. For instance, the NPT simulation with $\tau_T = 20$ ps is labelled as NPT_Mrun_{T₂₀}. Furthermore, two additional

NVT simulations with sys-M were carried out, where different temperature control methods, Nosé–Hoover⁵⁴ (NVT_Mrun_{T2}) and velocity rescaling thermostats⁵⁵ (NVT_M) with τ_T of 2 ps, were applied. Additionally, one NVT trajectory (labelled as Hybrid_M), was performed with sys-M where a thermostat with $\tau_T = 2$ ps was coupled only with the H₂S species at 250 K, leaving the H₂O species without direct temperature control (see Table S1).

The TIP4P/Ice potential was applied for water,⁵⁷ and a four-site potential proposed by Forester *et al.* was applied for H₂S,⁵⁸ with the H–S bond of 0.134 nm. All molecular models are rigid. Additional methodological details are presented in the supplementary material.

To track hydrate formation, both F₄ order parameters^{59,60} (which quantify the hydrate-like arrangements of water molecules) and hydrate cages with their corresponding occupancy (as measured by a modified FSICA code⁶¹) were used. The average F₄ values for crystalline hydrate structures (i.e., of sI and sII) is 0.7, while for liquid water is −0.04.^{59,60} To explore heat transfer and hence local temperature variations as hydrate formation proceeds, various temperature measures were determined from the kinetic energies of the molecules. The configurations were collected with a sampling time of 20 ps for temperature measurement. The temperature of the entire system, T_{sys} , is given by

$$T_{sys} = \frac{1}{N} \sum_i^N T_i \quad (1)$$

where N is the total number of molecules in the system, and T_i obtained from $T_i = \frac{2}{N_{df,i} k_b} E_{kin,i}$, in which $E_{kin,i}$ is the total kinetic energy of the molecule i , $N_{df,i} = 6$ is the number of degrees of freedom of the molecule i , and k_b is the Boltzmann constant. Note here we have made no provision for missing/constrained degree of freedom of the system, although the correction will be very small for the present systems. Similarly, the temperature for the water species is given by

$$T_{wat} = \frac{1}{N_{wat}} \sum_i^{N_{wat}} T_i \quad (2)$$

where N_{wat} is the total number of water molecules in the system.

The spatial distribution for the temperature is also of interest. To generate the spatial distribution, the system box was partitioned into $7 \times 7 \times 7$ (343) cubic cells, as illustrated in Fig. 1, where, for example, each cubic cell has a length of ∼1.26 nm and a volume of ∼2 nm³ for NVE sys-M systems. We note that for systems within the NPT simulations, the size of each cubic cell is allowed to vary slightly, scaling with the system size. The temperature for each cell, T_{cell} , can then be expressed as a weighted average over all molecules in the cell:

$$T_{cell} = \frac{\sum_i T_i w_i}{\sum_i w_i} \quad (3)$$

where w_i is the fraction of the atoms in the molecule in the particular cell. For example, if two atoms for a H₂S molecule are detected in the cell, w_i would be 2/3. The temperature for the entire system, T_{sys} , given in Eq. (1) can alternatively be expressed as

$$T_{sys} = \frac{1}{N_{cell}} \sum_{cell}^{N_{cell}} T_{cell} \quad (4)$$

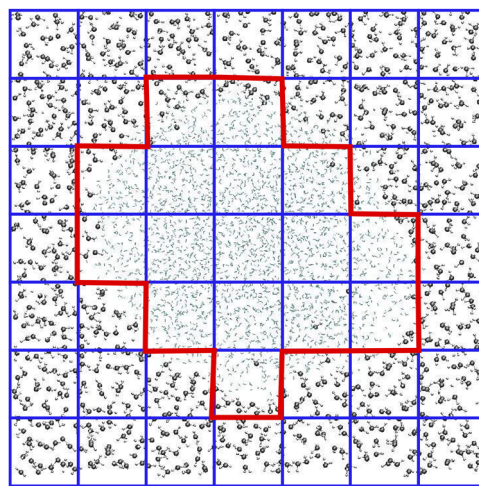


FIG. 1. 2D schematic representation for cubic cells partitioned from a configuration of sys-M. The liquid H₂O molecules are shown by gray lines. The H₂S molecules in bulk non-aqueous phase are represented by gray (S-atom) and white (H-atom) spheres. The blue lines indicate boundaries for the cubic cells. The red lines indicate the cells counted as part of the nanodroplet region.

where $N_{cell} = 343$ is the total number of cells in the system. Analogous to the definition of T_{sys} in Eq. (4), we can define T_{drop} for the temperature of the nanodroplet region based on T_{cell} , namely,

$$T_{drop} = \frac{1}{N_{cell,drop}} \sum_{cell,drop}^{N_{cell,drop}} T_{cell} \quad (5)$$

where $N_{cell,drop}$ is the number of cells belonging to the nanodroplet region (typically in the range of ∼55–68). A cubic cell is categorized as being part of the nanodroplet region if it contains more than 25 water molecules, which corresponds to about 40% of the usual number of water molecules in cubic cells within the bulk water region (see Fig. 1). It is noteworthy that the temperatures obtained for the cubic cells in each configuration exhibit rather large fluctuations given the relatively small number of molecules (less than 70) in each cell. To

TABLE I. Average induction time (ns) for the nucleation from both NPT and NVE simulations.^a

Ensemble	Sys-M ($T_0 = 250$ K)	Sys-M ($T_0 = 255$ K)	Sys-L ($T_0 = 255$ K)
NVE	276(141)	...	911 ^c
NPT ^d	95(49)	161(83)	154(74)

^aInduction time is defined as the first time when more than two persistent complete cages appear.³¹ The values of standard deviations are given in parentheses.

^bNo nucleation events were observed for a total of 2.5 μ s simulation time from five trajectories.

^cOnly 2 out of 5 trajectories exhibit nucleation events (see Fig. S1).

^dValues from Ref. 31.

reduce the statistical noise associated with the cell temperature, an average over a specific time window for T_{cell} was determined as

$$\langle T_{cell} \rangle_{\tau} = \frac{1}{N_{\tau}} \sum_{i=1}^{N_{\tau}} T_{cell,i} \quad (6)$$

where N_{τ} is the total number of configurations collected within the time window τ . If the case of $N_{\tau} = 50$ is considered, with sampling

every 20 ps, the temperature for the cell was averaged over 1 ns and labelled as $\langle T_{cell} \rangle_{1ns}$.

RESULTS AND DISCUSSION

Since nucleation events were observed in all sys-M trajectories for the NVE simulations with $T_0 = 250$ K, as shown in Table I,

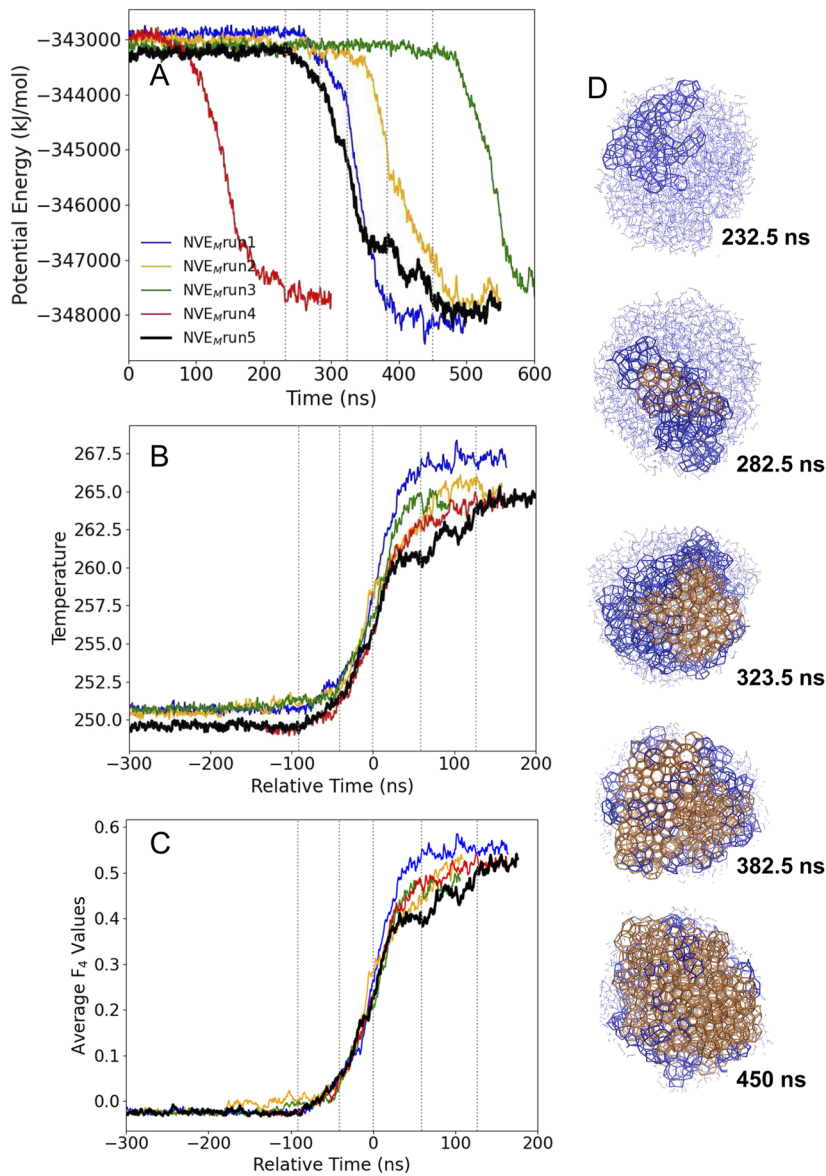


FIG. 2. Nucleation process for sys-M from NVE trajectories for $T_0 = 250$ K (NVE_M). (a) Time evolution of potential energy for each trajectory. (b) Time evolution of the temperature. (c) Time evolution of the average F_4 values. In panels (b) and (c), the relative time scales^{29–31,62} were used (detailed in the main text). Panels (a)–(c) use the same color scheme. (d) Snapshots of the largest hydrate cluster taken at various stages from the nucleation process in a typical trajectory, run 5, highlighted by the heavy dark line in panels (a)–(c). Standard (std) cages⁶¹ are colored in brown and other cages are colored in blue. The liquid water molecules are represented by blue lines. H₂S molecules in water cages and the liquid H₂S phase are omitted for visual clarity. In panels (a)–(c), the dashed lines correspond to the time points of the snapshots in panel (d).

Figs. 2 and S1, our detailed analysis will focus on these trajectories (i.e., NVE_{Mrun1–5}). The expected warming and decrease in potential energy for the entire system within these NVE simulations, as hydrate nucleation and growth proceed, are captured in Fig. 2. Initially the potential energy, temperature and F₄ fluctuate around their initial values during the quiescent period. Signaled by a decrease in potential energy and increases in the temperature and F₄ values in Fig. 2, the phase conversion from aqueous solutions to hydrate-like solids proceeds until the values of all three variables level off near the end of the simulated trajectories, indicating that essentially the entire water nanodroplet has become a hydrate-like solid [see Fig. 2(d)]. We note that the time scale used for the temporal alignment, i.e., in Figs. 2(b) and 2(c), is the relative time where the time points were shifted by setting the time corresponding to the inflection points of the fitted sigmoidal function for F₄ values to zero.^{29–31,62}

To investigate the possible influence of temperature control schemes on nucleation behavior, the results from previous NPT simulations³¹ with the same system set-up, the same models, and the same conditions have been compared, and nucleation behavior within these previous NPT simulations is shown in Figs. S2 and S3. Consistent with previous studies,^{37,40} the observed nucleation behavior from the NVE and NPT simulations exhibits strong similarities, yet these simulations also give different formation rates and different ratios for standard cages, as shown in Figs. 2, S2, and S3.³¹ Independent of the simulations, the nucleation process is consistently observed to be initiated by the advent of defective (i.e., irregular) cages. Then more regular cages (also called standard cages)^{29,31} arise apparently from such defective cages until the transition process concludes with almost the entire water nanodroplet being converted into hydrate-like, but still amorphous, solids (see Figs. 2 and S2). However, we see from Table I that the nucleation rate from the NVE simulations is ~3 times slower than that observed from the NPT simulations for sys-M and T₀ of 250 K. The reduction of the nucleation rate for NVE simulations is even more pronounced with a temperature T₀ of 255 K and for a larger water nanodroplet (sys-L), as shown in Table I. On the other hand, the growth rate is enhanced within the NVE simulations, indicated by a faster increase in the average F₄ values (i.e., a steeper curve close to relative time = 0, when ordering rates are a maximum), as shown in Fig. 3.

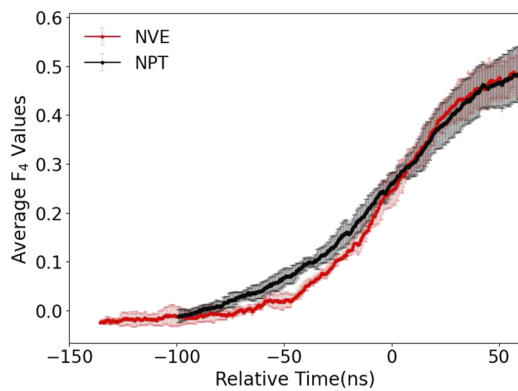


FIG. 3. Comparison for average F₄ values from temporally aligned curves for NVE and NPT³¹ simulations with sys-M, where the standard deviations for each are provided.

Additionally, NVE simulations exhibit a lower ratio of 5¹²/5¹² 6² cages along with a lower proportion of other cages (see Fig. S3) indicating better overall hydrate structure. In NVE simulations, the system is heated as hydrate formation proceeds, and this heating in turn allows for faster dynamics and rearrangement into more crystalline structures. However, during the quiescent period, the temperatures of both NVE and NPT systems fluctuate around the same initial value, yet the measured induction times appear impacted by whether a temperature control scheme is applied. This leads us to conjecture whether differences in the characteristics of the temperature fluctuations during the quiescent period might be responsible. To explore this question, probability distributions as well as spatial distributions for the temperature will be investigated.

Before proceeding, however, it is useful first to consider the guest concentration as it is a critical factor that can alter hydrate nucleation rates.^{15,27,31,63} The concentration of H₂S in the aqueous nanodroplet prior to nucleation was measured for the NVE and NPT systems and was found to be essentially constant across all systems and with different temperature coupling strengths (see Table II). Additionally, the fluctuations in the local concentration of H₂S for the quiescent period and early stage of hydrate nucleation were examined, and typical results are presented in Fig. S4. We find that prior to nucleation, there is no consistent pattern in the local concentration fluctuations. It is noteworthy that the local concentration of H₂S must inevitably increase during hydrate formation (as shown in Fig. S5), since the local concentration of H₂S is about 0.15 (mole fraction) in a hydrate crystallite, which is considerably larger than that in solution. However, we find that the increase in the local concentration tends to coincide with the formation of the hydrate nucleus rather than proceeding it. These results then indicate that the guest concentration can be ruled out as a possible factor responsible for the NVE-suppressed nucleation rate.

The probability distributions for the instantaneous temperature, P(T), from thermostatted systems should provide canonical distributions for both the entire system and any subsystem (e.g., water), and can be approximated as a Gaussian distribution when the number of degrees of freedom is large.⁶⁴ Since the average temperatures for thermostatted systems have been constrained, their temperature distributions were determined from the whole trajectory (shown in Fig. S6) with the exclusion of the first 1 ns of the simulation, while the temperature distributions from the NVE trajectories were determined from the quiescent period prior to the temperature increase due to nucleation. As exemplified in Fig. 4(a), a clear difference in the widths of P(T) for T_{sys} unsurprisingly exists from thermostatted and NVE simulations. This can be understood

TABLE II. Concentration of H₂S in the cores of the water nanodroplets prior to the nucleation.^a

System	H ₂ S
NVE _{Mrun5}	0.060 (0.004)
NPT _{Mrun_{T20}}	0.065 (0.002)
Run 6 from NPT simulations ^b	0.064 (0.004)

^aThe concentration of H₂S in the cores of the water nanodroplets.³¹ at 250 K for each system is considered, where the molar fraction was determined from a 50 to 100 ns window in the trajectory. The standard deviation has been provided in parenthesis.

^bThis trajectory is presented as the brown curve in Figs. S2(a) and S2(b).

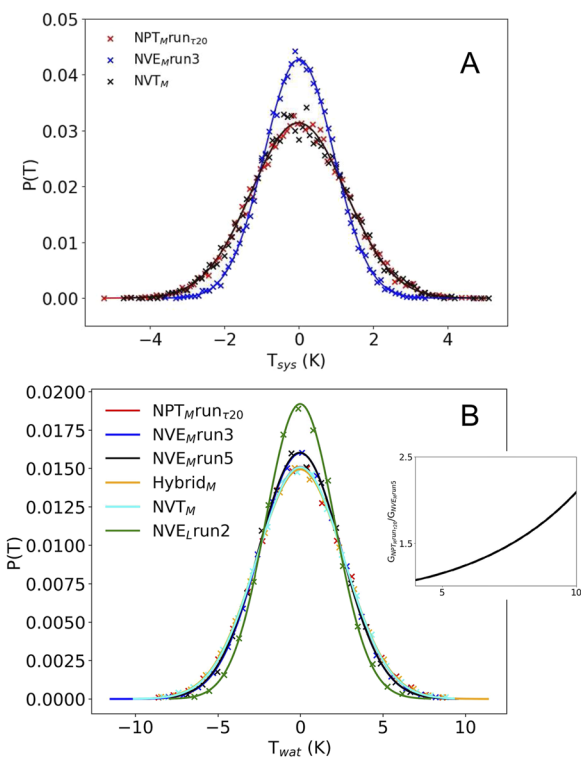


FIG. 4. Probability distributions, $P(T)$, of instantaneous temperature: (a) for the entire system, T_{sys} , and (b) for water species, T_{wat} . In panels (a) and (b), the mean values of the distributions have been shifted to zero. For the NVE simulations, data was collected over time windows before nucleation occurs [i.e., from 1 to 400 ns in NVE_{Mrun3} and from 1 to 200 ns in NVE_{Mrun5} , the green and the black curve in Figs. 2(a)–2(c), respectively; from 1 to 300 ns in NVE_{Lrun2} , the yellow curve in Fig. S1]. For each NPT, NVT and Hybrid_M trajectory, a 350 ns time window was used. The representative NVT_M trajectory is the one thermostatted by the velocity rescaling method.⁵⁶ In both panels (a) and (b), the fitted Gaussian to each distribution is presented as the solid curve and data points are shown by cross symbols, where in panel (a) the original point spacing of 0.1 K is used and in panel (b) points have been smoothed over a 0.9 K bin-size. To confirm the Gaussian fit performance for T_{wat} , the data points with the original 0.1 K spacing and the smoothed 0.9 K points are compared in Fig. S7 for a representative data set. The inset in panel (b) shows a plot of the ratio of the Gaussian fit probabilities, G , between $NPT_{Mrun\tau20}$ and NVE_{Mrun5} for the tail region of the curve.

by realizing that a NVE system is constrained to sample phase space at a fixed value of the total energy, while a thermostatted system samples a range of total energies consistent with a specific value of temperature.⁶⁵ Consequently, the NVE system should exhibit a narrower temperature distribution. We can see in Fig. 4(a) that the thermostatted systems, $NPT_{Mrun\tau20}$ and NVT_M , obeying the canonical distribution,⁶⁴ have a wider $P(T)$ for T_{sys} , with $\sigma = 1.27 \pm 0.01$ for both thermostats, in comparison with $\sigma = 0.93 \pm 0.005$ for NVE_{Mrun3} . Similar values of σ , specifically 0.96 ± 0.04 , were obtained for the other NVE_M trajectories (where NVE_{Mrun4} with its rather short quiescent period was not taken into consideration). It should also be noted that smaller values of τ_T , namely $\tau_T \leq 10$ ps, for Nosé–Hoover thermostat give somewhat larger σ values for $P(T)$ for

T_{sys} (e.g., $\sigma = 1.41$ for $\tau_T = 2$ ps). Hence, when a Nosé–Hoover thermostat is applied, a larger value of τ_T should be used to achieve the correct canonical temperature distribution. We also remark that the presence of pressure control in thermostatted simulations appears to leave the probability distributions of the system temperature unchanged, as expected.

It is also interesting and important to consider the temperature distribution for the subsystem composed of only the water molecules. Since the number of water molecules in the current systems is much less than the total number of molecules, broader distributions and larger values of σ for $P(T)$ of T_{wat} are expected in comparison with those for T_{sys} (see Fig. 4). Probability distributions for T_{wat} for two representative NVE simulations (i.e., NVE_{Mrun3} and NVE_{Mrun5}), and two representative thermostatted simulations (i.e., $NPT_{Mrun\tau20}$ and NVT_M) are presented in Fig. 4(b). It is apparent from Fig. 4(b) that there is a distinguishable difference in the σ values from the thermostatted and NVE simulations. The average values of σ are 2.65 ± 0.02 for the thermostatted systems, and 2.51 ± 0.03 for the NVE systems. As shown in the inset of Fig. 4(b), the ratio of the probabilities from the Gaussian fits for $NPT_{Mrun\tau20}$ and NVE_{Mrun5} increases and becomes significantly larger than 1 for the tails of these distributions. We conjecture that this difference in the temperature fluctuations for the constant energy and constant temperature simulations allows the water molecules in thermostatted systems to experience an enhanced sampling of higher and lower temperatures, where the latter may enhance the formation of hydrate nuclei.

This difference between constant temperature and constant energy simulations can be arguably attributed to a finite-size effect. We can understand this effect by utilizing the schematic model shown in Fig. 5. The current system can be seen to be made up of two subsystems: a discrete water nanodroplet and a surrounding H_2S liquid. Within an NPT system, the temperature of both H_2S and H_2O molecules are controlled directly through the coupling to the external thermal bath, represented by the blue region in Fig. 5. Within an NVE system, there is only coupling between the temperatures of the H_2O subsystem to those of the H_2S subsystem, represented by the red part in Fig. 5. Because of its much larger size, the H_2S subsystem can serve as a finite-size thermal bath surrounding the water

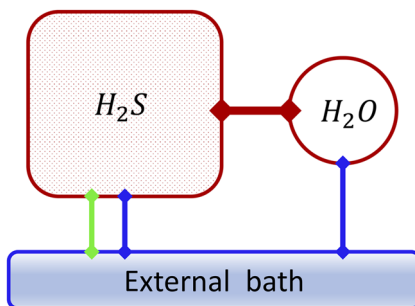


FIG. 5. Schematic representation for heat flow and temperature coupling between the H_2S and H_2O sub-systems for an NVE system (the red components only), and between the two sub-systems and an external thermal bath for an NPT system (the red and blue components). For a Hybrid_M system, the green arrow represents the coupling of only the H_2S subsystem to the external thermal bath.

nanodroplet. It is then possible to attribute the difference in $P(T)$ for T_{wat} obtained in Fig. 4(b) for NPT and NVE simulations to a finite-size effect (i.e., due to the limited size of the H₂S “bath”). If one could significantly enlarge the size of the H₂S subsystem, the difference in the fluctuations in the water subsystem observed from NPT and NVE simulations should vanish. We can validate this conjecture in two ways. First, we have performed a Hybrid_M simulation, where only the temperature of the H₂S molecules is coupled to the external

bath (as captured by the green arrow in Fig. 5) to mimic an infinite H₂S subsystem. If the conjecture is correct, then $P(T)$ for T_{wat} of the Hybrid_M will be broader in comparison with that from the NVE simulations and be the same width as from the NPT simulations. Secondly, an increase in the size of the water nanodroplet relative to the H₂S liquid should result in a smaller σ value for $P(T)$ for T_{wat} and hence a narrower distribution. The $P(T)$ distributions for T_{wat} shown in Fig. 4(b) and their corresponding values of σ validate this

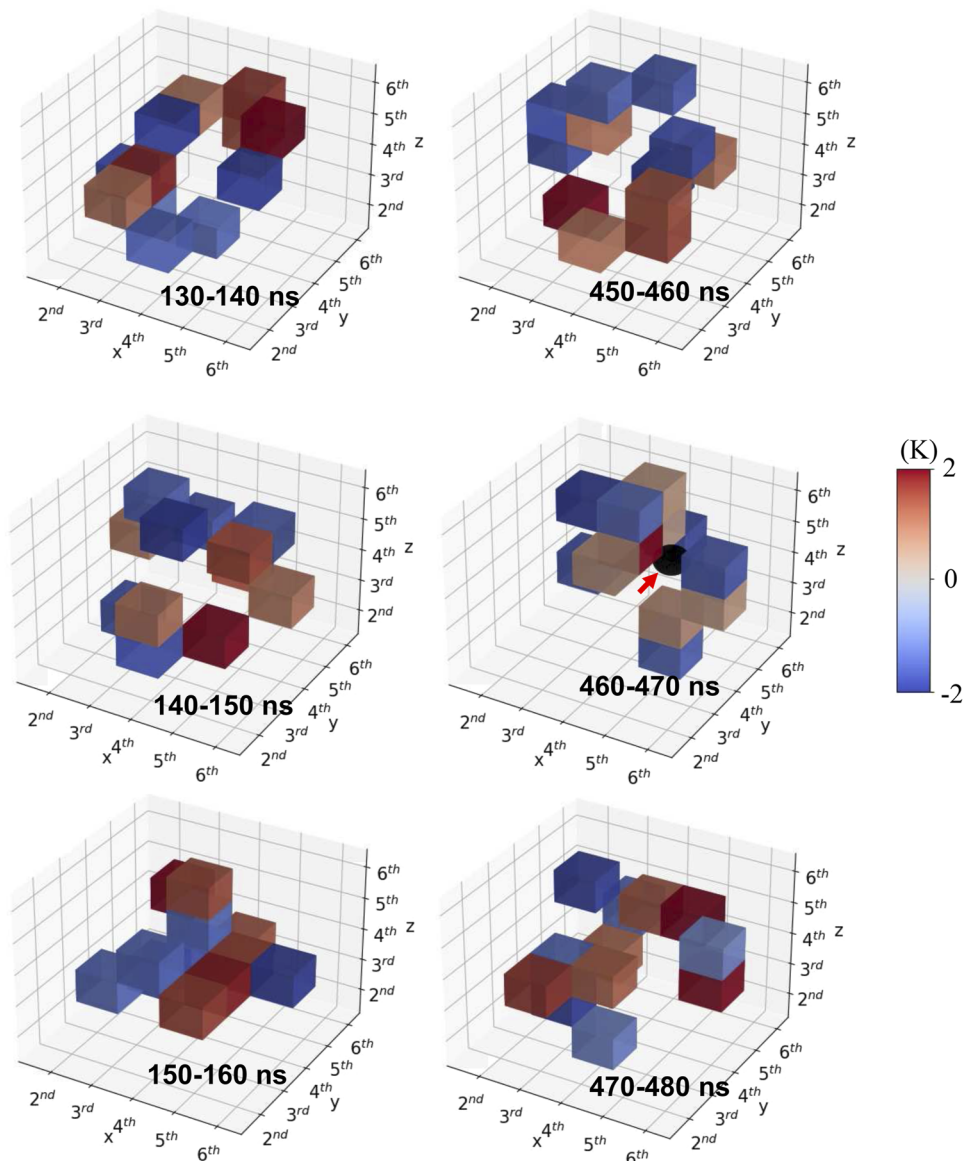


FIG. 6. Representative examples of the spatial distribution of $\langle T_{\text{cell}} \rangle_{10\text{ns}}$ in the water nanodroplet region in which only the six hottest and the six coldest cubic cells are presented. The temperature for each cell is the average value over a 10 ns interval from NVE_Mrun3, the green curve in Fig. 2. Spatial distributions from the quiescent period (left column) and the early stage of hydrate nucleation (right column) have been presented where the induction time for the current simulation trajectory is 465 ns. The mean value from the fitted Gaussian to the distribution in terms of $\langle T_{\text{cell}} \rangle_{10\text{ns}}$ has been shifted to zero. The approximate location of the hydrate nucleus at 465 ns, pointed out by a red arrow, is represented by a black sphere with a radius of 0.5 nm in the plot for 460–470 ns.

conjecture. Namely, values of σ are equal to 2.51 ± 0.03 for NVE_M, yet equal to 2.64 ± 0.01 for Hybrid_M, 2.08 ± 0.02 for NVE_Lrun2, and 2.65 ± 0.02 for thermostatted systems. We note that the square root of the ratio of the numbers of water molecules in the NVE_L and NVE_M systems (which have the same number of molecules of H₂S) equals the reciprocal of the ratio of the respective σ values. Furthermore, the narrower distributions for $P(T)$ for T_{wat} in the NVE_L relative to the NVE_M simulations also lead to a greater impact on the nucleation rates for the former (see Table I).

Given the importance of the temperature coupling between H₂O and H₂S, it is also interesting to explore whether local (spatial) variations might develop during hydrate nucleation. For this purpose, possible local patterns in temperature were examined using spatial distributions, where two possible scenarios are considered. (1) The nucleus may arise at a locally colder place because of the strong temperature dependence of nucleation. In this case, a local minimum of the temperature may be monitored just prior to the appearance of the nucleus. (2) Alternatively, if there is no preferential temperature precondition enhancing the appearance of the nucleus, then as a result of the heat generated by nucleation, a local maximum value in the temperature might be apparent and thus be monitored as nucleation occurs. Therefore, a possible relationship between local hot or cold spots and the site of the initial nuclei should help demonstrate if either of these scenarios occurs. Using the definition for the temperature of cubic cells, T_{cell} [see Eqs. (3)–(6)], the spatial distribution of temperature can be monitored. 10 ns averaged values, $\langle T_{\text{cell}} \rangle_{10\text{ns}}$, are used to help reduce fluctuations in the values where the spatial profile for the temperature is monitored for the nanodroplet region.

Spatial distributions for $\langle T_{\text{cell}} \rangle_{10\text{ns}}$ in the nanodroplet region are presented in Fig. 6 where only the six hottest and the six coldest cells are shown. The apparent random patterns of the local hot/cold regions in the nanodroplet region for both the quiescent period and the early stage of hydrate nucleation provide no evidence supporting either of the two aforementioned scenarios. This is in apparent contrast to the previous work of Liang and Kusalik, where a slight temperature gradient of about 2 K was detected between the region of the initial nucleus and the surrounding aqueous solution.³⁷ However, it should be noted that the previous work³⁷ was performed under supersaturated and supercooled conditions where the nucleation and growth occurred very rapidly with a correspondingly rapid heat release rate. Therefore, this rapid rate of heat dissipation apparently resulted in the formation of a temperature gradient that could be captured.³⁷ However, for the current system the saturated solution and supercooled conditions lead to nucleation and subsequent growth occurring at a significantly slower rate, and thus the rate of heat dissipation is slower and the temperature gradient smaller. Consequently, temperature fluctuations dominate and only random patterns for the spatial distribution of T_{cell} are observed. We also note that the NVE-suppressed nucleation rate is apparently not the result of local temperature imbalance according to these results.

Despite no apparent spatial patterns in the local temperature distributions, the heat generated by hydrate formation must inevitably result in a temperature gradient in an NVE simulation to drive the spontaneous heat flow from the “hotter” nucleus to the “colder” surroundings. For this reason, we have monitored the temperature difference between the nanodroplet region and the entire system, the values of which are shown in Fig. 7. While the water

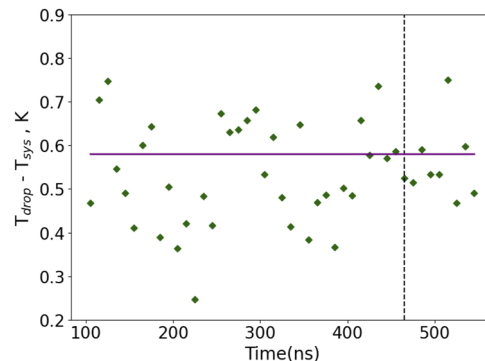


FIG. 7. Time evolution of the difference between the temperature for the water region and the temperature for the entire system averaged over 10 ns time windows from the NVE_Mrun3 trajectory. The differences between the mean value for the water region and that for the entire system are given as green diamonds. The purple line represents the intrinsic temperature difference between the temperature of the water species and the temperature of the entire system (see text for details). The dashed vertical line indicates the induction time of the current trajectory.

region is consistently slightly hotter than the system, the unphysical “hot solvent/cold solute” issue³⁶ (arising from numerical noise during the calculation of the water dynamics) exists in the simulation. This intrinsic temperature difference between the water species and the entire system is also shown by the purple line in Fig. 7. We find that the temperature difference between the nanodroplet region and the entire system fluctuates around the value of the intrinsic temperature difference both before and after nucleation. Additionally, fluctuations of a comparable magnitude were also present within NPT systems. Given these results, we conclude that the temperature gradient in the current NVE simulations was too small to be measured in this manner.

Finally, we can look to estimate the value of the temperature difference between the nanodroplet region and the rest of the system. We start with a model where the water nanodroplet region is the heat “source” and the H₂S phase region is the heat “bath,” and consider the thermal conductivity as given by Fourier’s law

$$\frac{\Delta Q}{\Delta t} = -\kappa A \frac{\Delta T_X}{\Delta X} \quad (7)$$

where κ is the thermal conductivity of liquid H₂S, $A = 4\pi R^2$ is the area of the sphere with radius R enclosing the region containing the hydrate nucleus, and $\Delta T_X/\Delta X$ is the temperature gradient across the boundary of the sphere. In Eq. (7), ΔQ is the total heat released during the elapsed time Δt due to hydrate formation; it can be approximated by $nC_{P,m,\text{H}_2\text{S}(l)}\Delta T_t$ in which n is moles of H₂S in the system, $C_{P,m,\text{H}_2\text{S}(l)}$ is the heat capacity of H₂S liquid, and ΔT_t is the temperature change over the time Δt . Taking the rate of temperature change for sys-M from NVE simulations at $T_0 = 250$ K [see Fig. 2(b)], together with $R = 2$ nm,³¹ yields an estimate of 10^{-2} K/nm for $\Delta T_X/\Delta X$, confirming that the expected temperature gradient should be quite small.

CONCLUSIONS

In this study, extensive NVE and thermostatted simulations of systems consisting of a H₂O nanodroplet immersed in a H₂S liquid were performed, and the influence of the temperature control schemes, and temperature coupling strengths and coupling groups upon the hydrate nucleation behavior were examined. Detailed analysis of the hydrate structures and their formation mechanisms revealed similar overall behavior for the NVE and NPT simulations. Consistent with previous studies, the NVE simulations were found to exhibit a slower nucleation rate yet a faster growth rate of nuclei with more recognizable crystal features in comparison with those found from NPT simulations. To probe the origins of the difference in nucleation rates, probability and spatial distributions for various temperature measures were examined. Through comparison of the temperature distributions obtained, a small yet detectable difference in the widths of the water temperature distributions was observed. The somewhat reduced fluctuations in the temperature for the water species in the NVE simulations appear to be responsible for reducing the hydrate nucleation rate. We conjecture the NVE-impeded nucleation rate may be attributed to the finite size of the surroundings (here the liquid H₂S portion of the system) which implies that the effect should diminish as the size of the surrounding region becomes large. In addition, a local temperature gradient, arising from the large amount of heat released during hydrate formation, could not be detected (relative to the intrinsic noise of the NVE simulation data); a rather small magnitude for this gradient, roughly 0.01 K/nm, can be estimated from the observed heating rate of the current NVE simulations. While the conditions in the present study correspond to those more typically seen in experiments exploring gas hydrate nucleation, different conditions or different systems that might feature more rapid heating rates can be expected to exhibit more significant temperature gradients.

SUPPLEMENTARY MATERIAL

Additional details of methodologies and supplementary figures for the nucleation process are provided in the supplementary material. Figures for the local centration of H₂S in the cores of the water nanodroplets, and for confirming the performance of the Gaussian fit for T_{wat} are also provided in supplementary material.

ACKNOWLEDGMENTS

We are grateful for the financial support of the Natural Sciences and Engineering Research Council of Canada (Grant No. RGPIN-2022-03549). We thank Compute Canada for its computational resources. We also thank Dr. Zhengcui Zhang for providing access to a modified version of the FSICA code and for helpful discussions regarding NVE simulations.

AUTHOR DECLARATIONS

Conflict of Interest

The authors have no conflicts to disclose.

Author Contributions

Lei Wang: Conceptualization (supporting); Data curation (lead); Formal analysis (equal); Investigation (lead); Methodology (equal); Resources (equal); Software (lead); Validation (equal); Visualization (lead); Writing – original draft (lead); Writing – review & editing (equal). **Peter G. Kusalik:** Conceptualization (lead); Data curation (supporting); Formal analysis (equal); Funding acquisition (lead); Investigation (supporting); Methodology (equal); Project administration (lead); Resources (equal); Software (supporting); Supervision (lead); Validation (equal); Visualization (supporting); Writing – original draft (supporting); Writing – review & editing (equal).

DATA AVAILABILITY

The data that support the findings of this study are available from the corresponding author upon reasonable request.

REFERENCES

- ¹E. D. Sloan, C. A. Koh, and C. Koh, *Clathrate Hydrates of Natural Gases* (CRC Press, Boca Raton, FL, 2007).
- ²M. Kastner, M. Myers, C. A. Koh, G. Moridis, J. E. Johnson, and J. Thurmond, “Energy transition and climate mitigation require increased effort on methane hydrate research,” *Energy Fuels* **36**(6), 2923–2926 (2022).
- ³Z. Yin and P. Linga, “Methane hydrates: A future clean energy resource,” *Chin. J. Chem. Eng.* **27**(9), 2026–2036 (2019).
- ⁴J. L. Wadham, S. Arndt, S. Tulaczyk, M. Stibal, M. Tranter, J. Telling, G. P. Lis, E. Lawson, A. Ridgwell, A. Dubnick, M. J. Sharp, A. M. Anesio, and C. E. H. Butler, “Potential methane reservoirs beneath Antarctica,” *Nature* **488**(7413), 633–637 (2012).
- ⁵Y.-S. Yu, X. Zhang, J.-W. Liu, Y. Lee, and X.-S. Li, “Natural gas hydrate resources and hydrate technologies: A review and analysis of the associated energy and global warming challenges,” *Energy Environ. Sci.* **14**(11), 5611–5668 (2021).
- ⁶M. Khurana, Z. Yin, and P. Linga, “A review of clathrate hydrate nucleation,” *ACS Sustainable Chem. Eng.* **5**(12), 11176–11203 (2017).
- ⁷A. Hassanpourouzband, E. Joonaki, M. Vasheghani Farahani, S. Takeya, C. Ruppel, J. Yang, N. J. English, J. M. Schicks, K. Edlmann, H. Mehrabian, Z. M. Aman, and B. Tohidi, “Gas hydrates in sustainable chemistry,” *Chem. Soc. Rev.* **49**(15), 5225–5309 (2020).
- ⁸Z. Cheng, S. Li, Y. Liu, Y. Zhang, Z. Ling, M. Yang, L. Jiang, and Y. Song, “Post-combustion CO₂ capture and separation in flue gas based on hydrate technology: A review,” *Renewable Sustainable Energy Rev.* **154**, 111806 (2022).
- ⁹H. P. Veluswamy, A. Kumar, Y. Seo, J. D. Lee, and P. Linga, “A review of solidified natural gas (SNG) technology for gas storage via clathrate hydrates,” *Appl. Energy* **216**, 262–285 (2018).
- ¹⁰M. Khan, P. Warrier, C. Peters, and C. Koh, “Hydrate-based separation for industrial gas mixtures,” *Energies* **15**(3), 966 (2022).
- ¹¹H. Dong, J. Wang, Z. Xie, B. Wang, L. Zhang, and Q. Shi, “Potential applications based on the formation and dissociation of gas hydrates,” *Renewable Sustainable Energy Rev.* **143**, 110928 (2021).
- ¹²P. Babu, A. Nambiar, T. He, I. A. Karimi, J. D. Lee, P. Englezos, and P. Linga, “A review of clathrate hydrate based desalination to strengthen energy-water nexus,” *ACS Sustainable Chem. Eng.* **6**(7), 8093–8107 (2018).
- ¹³B. Shi, S. Song, Y. Chen, X. Duan, Q. Liao, S. Fu, L. Liu, J. Sui, J. Jia, H. Liu, Y. Zhu, C. Song, D. Lin, T. Wang, J. Wang, H. Yao, and J. Gong, “Status of natural gas hydrate flow assurance research in China: A review,” *Energy Fuels* **35**(5), 3611–3658 (2021).
- ¹⁴G. C. Sosso, J. Chen, S. J. Cox, M. Fitzner, P. Pedevilla, A. Zen, and A. Michaelides, “Crystal nucleation in liquids: Open questions and future challenges in molecular dynamics simulations,” *Chem. Rev.* **116**(12), 7078–7116 (2016).

- ¹⁵J. Grabowska, S. Blazquez, E. Sanz, I. M. Zerón, J. Algaba, J. M. Míguez, F. J. Blas, and C. Vega, "Solubility of methane in water: Some useful results for hydrate nucleation," *J. Phys. Chem. B* **126**(42), 8553–8570 (2022).
- ¹⁶M. R. Ghaani, C. C. R. Allen, T. Skvortsov, and N. J. English, "Engineering peptides to catalyze and control stabilization of gas hydrates: Learning from nature," *J. Phys. Chem. Lett.* **11**(13), 5068–5075 (2020).
- ¹⁷G.-J. Guo, P. M. Rodger, and P. Mark Rodger, "Solubility of aqueous methane under metastable conditions: Implications for gas hydrate nucleation," *J. Phys. Chem. B* **117**(21), 6498–6504 (2013).
- ¹⁸B. C. Knott, V. Molinero, M. F. Doherty, and B. Peters, "Homogeneous nucleation of methane hydrates: Unrealistic under realistic conditions," *J. Am. Chem. Soc.* **134**(48), 19544–19547 (2012).
- ¹⁹S. Sarupria and P. G. Debenedetti, "Homogeneous nucleation of methane hydrate in microsecond molecular dynamics simulations," *J. Phys. Chem. Lett.* **3**(20), 2942–2947 (2012).
- ²⁰M. R. Walsh, G. T. Beckham, C. A. Koh, E. D. Sloan, D. T. Wu, and A. K. Sum, "Methane hydrate nucleation rates from molecular dynamics simulations: Effects of aqueous methane concentration, interfacial curvature, and system size," *J. Phys. Chem. C* **115**(43), 21241–21248 (2011).
- ²¹M. R. Walsh, J. D. Rainey, P. G. Lafond, D.-H. Park, G. T. Beckham, M. D. Jones, K.-H. Lee, C. A. Koh, E. D. Sloan, D. T. Wu, and A. K. Sum, "The cages, dynamics, and structuring of incipient methane clathrate hydrates," *Phys. Chem. Chem. Phys.* **13**(44), 19951 (2011).
- ²²L. C. Jacobson and V. Molinero, "Can amorphous nuclei grow crystalline clathrates? The size and crystallinity of critical clathrate nuclei," *J. Am. Chem. Soc.* **133**(16), 6458–6463 (2011).
- ²³L. C. Jacobson, W. Hujo, and V. Molinero, "Amorphous precursors in the nucleation of clathrate hydrates," *J. Am. Chem. Soc.* **132**(33), 11806–11811 (2010).
- ²⁴M. R. Walsh, C. A. Koh, E. D. Sloan, A. K. Sum, and D. T. Wu, "Microsecond simulations of spontaneous methane hydrate nucleation and growth," *Science* **326**(5956), 1095–1098 (2009).
- ²⁵Z. He, K. M. Gupta, P. Linga, and J. Jiang, "Molecular insights into the nucleation and growth of CH₄ and CO₂ mixed hydrates from microsecond simulations," *J. Phys. Chem. C* **120**(44), 25225–25236 (2016).
- ²⁶Q. Liao, B. Shi, S. Li, S. Song, Y. Chen, J. Zhang, H. Yao, Q. Li, and J. Gong, "Molecular dynamics simulation of the effect of wax molecules on methane hydrate formation," *Fuel* **297**, 120778 (2021).
- ²⁷Z. Zhang, P. G. Kusalik, and G.-J. Guo, "Bridging solution properties to gas hydrate nucleation through guest dynamics," *Phys. Chem. Chem. Phys.* **20**(38), 24535–24538 (2018).
- ²⁸Z. He, K. Zhang, and J. Jiang, "Formation of CH₄ hydrate in a mesoporous metal-organic framework MIL-101: Mechanistic insights from microsecond molecular dynamics simulations," *J. Phys. Chem. Lett.* **10**(22), 7002–7008 (2019).
- ²⁹K. W. Hall, Z. Zhang, and P. G. Kusalik, "Unraveling mixed hydrate formation: Microscopic insights into early stage behavior," *J. Phys. Chem. B* **120**(51), 13218–13223 (2016).
- ³⁰L. Wang, K. Hall, Z. Zhang, and P. Kusalik, "Mixed hydrate nucleation: Molecular mechanisms and cage structures," *J. Phys. Chem. B* **126**(36), 7015–7026 (2022).
- ³¹L. Wang, Z. Zhang, and P. G. Kusalik, "Hydrate nucleation in water nanodroplets: Key factors and molecular mechanisms," *Energy Fuels* **37**(2), 1044–1056 (2023).
- ³²D. W. Kang, W. Lee, Y.-H. Ahn, and J. W. Lee, "Exploring tuning phenomena of THF-H₂ hydrates via molecular dynamics simulations," *J. Mol. Liq.* **349**, 118490 (2022).
- ³³Z. Zhang, G.-J. Guo, N. Wu, and P. G. Kusalik, "Molecular insights into guest and composition dependence of mixed hydrate nucleation," *J. Phys. Chem. C* **124**(45), 25078–25086 (2020).
- ³⁴M. M. Conde, M. A. Gonzalez, J. L. F. Abascal, and C. Vega, "Determining the phase diagram of water from direct coexistence simulations: The phase diagram of the TIP4P/2005 model revisited," *J. Chem. Phys.* **139**(15), 154505 (2013).
- ³⁵Z. Zhang, P. G. Kusalik, and G.-J. Guo, "Might a 2,2-dimethylbutane molecule serve as a site to promote gas hydrate nucleation?" *J. Phys. Chem. C* **123**(33), 20579–20586 (2019).
- ³⁶P. Naullage, A. A. Bertolazzo, and V. Molinero, "How do surfactants control the agglomeration of clathrate hydrates?", *ACS Cent. Sci.* **5**(3), 428–439 (2019).
- ³⁷S. Liang and P. G. Kusalik, "Nucleation of gas hydrates within constant energy systems," *J. Phys. Chem. B* **117**(5), 1403–1410 (2013).
- ³⁸Y. Bi, A. Porras, and T. Li, "Free energy landscape and molecular pathways of gas hydrate nucleation," *J. Chem. Phys.* **145**(21), 211909 (2016).
- ³⁹Z. Zhang, M. R. Walsh, and G. J. Guo, "Microcanonical molecular simulations of methane hydrate nucleation and growth: Evidence that direct nucleation to sI hydrate is among the multiple nucleation pathways," *Phys. Chem. Chem. Phys.* **17**(14), 8870–8876 (2015).
- ⁴⁰Z. Zhang, C.-J. Liu, M. R. Walsh, and G.-J. Guo, "Effects of ensembles on methane hydrate nucleation kinetics," *Phys. Chem. Chem. Phys.* **18**(23), 15602–15608 (2016).
- ⁴¹D. Yuhara, B. C. Barnes, D. Suh, B. C. Knott, G. T. Beckham, K. Yasuoka, D. T. Wu, and A. K. Sum, "Nucleation rate analysis of methane hydrate from molecular dynamics simulations," *Faraday Discuss.* **179**, 463–474 (2015).
- ⁴²M. Lauricella, S. Meloni, N. J. English, B. Peters, and G. Ciccotti, "Methane clathrate hydrate nucleation mechanism by advanced molecular simulations," *J. Phys. Chem. C* **118**(40), 22847–22857 (2014).
- ⁴³F. Jiménez-Ángeles and A. Firoozabadi, "Nucleation of methane hydrates at moderate subcooling by molecular dynamics simulations," *J. Phys. Chem. C* **118**(21), 11310–11318 (2014).
- ⁴⁴Y. Bi and T. Li, "Probing methane hydrate nucleation through the forward flux sampling method," *J. Phys. Chem. B* **118**(47), 13324–13332 (2014).
- ⁴⁵B. C. Barnes, B. C. Knott, G. T. Beckham, D. T. Wu, and A. K. Sum, "Reaction coordinate of incipient methane clathrate hydrate nucleation," *J. Phys. Chem. B* **118**(46), 13236–13243 (2014).
- ⁴⁶S. A. Aromada, B. Kvamme, N. Wei, and N. Saeidi, "Enthalpies of hydrate formation and dissociation from residual thermodynamics," *Energies* **12**(24), 4726 (2019).
- ⁴⁷G. K. Anderson, "Enthalpy of dissociation and hydration number of carbon dioxide hydrate from the Clapeyron equation," *J. Chem. Thermodyn.* **35**(7), 1171–1183 (2003).
- ⁴⁸S. Sun, Y. Hao, and J. Zhao, "Analysis of gas source for the replacement of CH₄ with CO₂ in gas hydrate production from the perspective of dissociation enthalpy," *J. Chem. Eng. Data* **63**(3), 684–690 (2018).
- ⁴⁹A. Gupta, J. Lachance, E. D. Sloan, and C. A. Koh, "Measurements of methane hydrate heat of dissociation using high pressure differential scanning calorimetry," *Chem. Eng. Sci.* **63**(24), 5848–5853 (2008).
- ⁵⁰I. N. Tsimplanogiannis, V. K. Michalis, and I. G. Economou, "Enthalpy of dissociation of methane hydrates at a wide pressure and temperature range," *Fluid Phase Equilib.* **489**, 30–40 (2019).
- ⁵¹C. A. Fuzo and L. Degrève, "Effect of the thermostat in the molecular dynamics simulation on the folding of the model protein chignolin," *J. Mol. Model.* **18**(6), 2785–2794 (2012).
- ⁵²K. W. Hall, S. Percec, and M. L. Klein, "Polymer nucleation under high-driving force, long-chain conditions: Heat release and the separation of time scales," *J. Chem. Phys.* **150**(11), 114901 (2019).
- ⁵³V. Tikkkanen, B. Reischl, H. Vehkämäki, and R. Halonen, "Nonisothermal nucleation in the gas phase is driven by cool subcritical clusters," *Proc. Natl. Acad. Sci. U. S. A.* **119**(28), e2201955119 (2022).
- ⁵⁴G. J. Martyna, M. L. Klein, and M. Tuckerman, "Nosé-Hoover chains: The canonical ensemble via continuous dynamics," *J. Chem. Phys.* **97**(4), 2635–2643 (1992).
- ⁵⁵M. Parrinello and A. Rahman, "Polymorphic transitions in single crystals: A new molecular dynamics method," *J. Appl. Phys.* **52**(12), 7182–7190 (1981).
- ⁵⁶G. Bussi, D. Donadio, and M. Parrinello, "Canonical sampling through velocity rescaling," *J. Chem. Phys.* **126**, 014101 (2007).
- ⁵⁷J. L. F. Abascal, E. Sanz, R. García Fernández, and C. Vega, "A potential model for the study of ices and amorphous water: TIP4P/Ice," *J. Chem. Phys.* **122**(23), 234511 (2005).
- ⁵⁸T. R. Forester, I. R. McDonald, and M. L. Klein, "Intermolecular potentials and the properties of liquid and solid hydrogen sulphide," *Chem. Phys.* **129**(2), 225–234 (1989).

- ⁵⁹P. M. Rodger, T. R. Forester, and W. Smith, "Simulations of the methane hydrate/methane gas interface near hydrate forming conditions," *Fluid Phase Equilib.* **116**(1–2), 326–332 (1996).
- ⁶⁰C. Moon, R. W. Hawtin, and P. M. Rodger, "Nucleation and control of clathrate hydrates: Insights from simulation," *Faraday Discuss.* **136**, 367–382 (2007).
- ⁶¹G.-J. Guo, Y.-G. Zhang, C.-J. Liu, and K.-H. Li, "Using the face-saturated incomplete cage analysis to quantify the cage compositions and cage linking structures of amorphous phase hydrates," *Phys. Chem. Chem. Phys.* **13**(25), 12048 (2011).
- ⁶²K. W. Hall, S. Carpendale, and P. G. Kusalik, "Evidence from mixed hydrate nucleation for a funnel model of crystallization," *Proc. Natl. Acad. Sci. U. S. A.* **113**(43), 12041–12046 (2016).
- ⁶³D. Kashchiev and A. Firoozabadi, "Driving force for crystallization of gas hydrates," *J. Cryst. Growth* **241**(1–2), 220–230 (2002).
- ⁶⁴M. Lingenheil, R. Denschlag, R. Reichold, and P. Tavan, "The 'hot-solvent/cold-solute' problem revisited," *J. Chem. Theory Comput.* **4**(8), 1293–1306 (2008).
- ⁶⁵K. Dill and S. Bromberg, *Molecular Driving Forces: Statistical Thermodynamics in Biology, Chemistry, Physics, and Nanoscience* (CRC Press, 2010).
- ⁶⁶K. Oda, H. Miyagawa, and K. Kitamura, "How does the electrostatic force cutoff generate non-uniform temperature distributions in proteins?", *Mol. Simul.* **16**(1–3), 167–177 (1996).